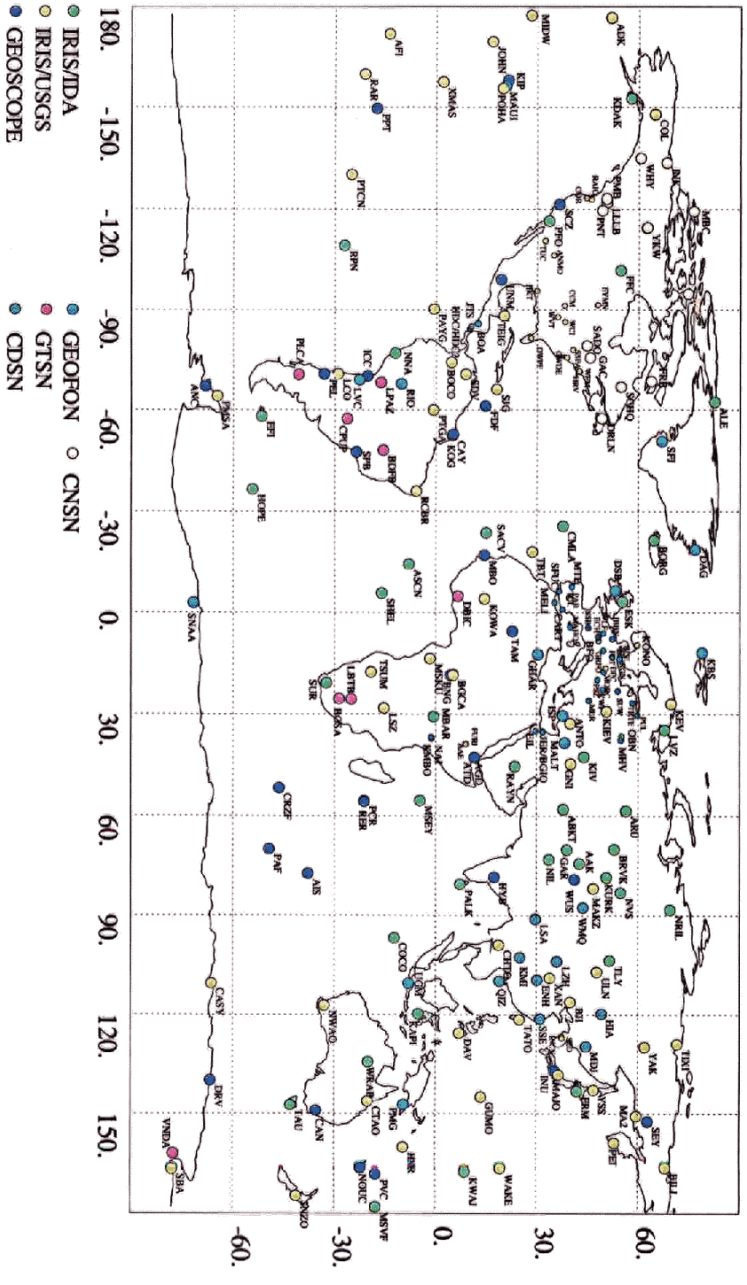

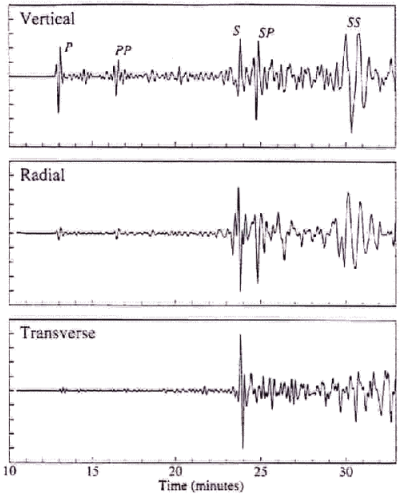

Fig. 4.16. The vertical, radial, and transverse components of ground motion (velocity) from the January 17, 1994 Northridge earthquake recorded at the IRIS/IDA station OBN at 88.5° range. The original broadband records have been filtered to between 15 and 100 s period. Time is in minutes relative to the earthquake origin time; amplitudes are self-scaled.

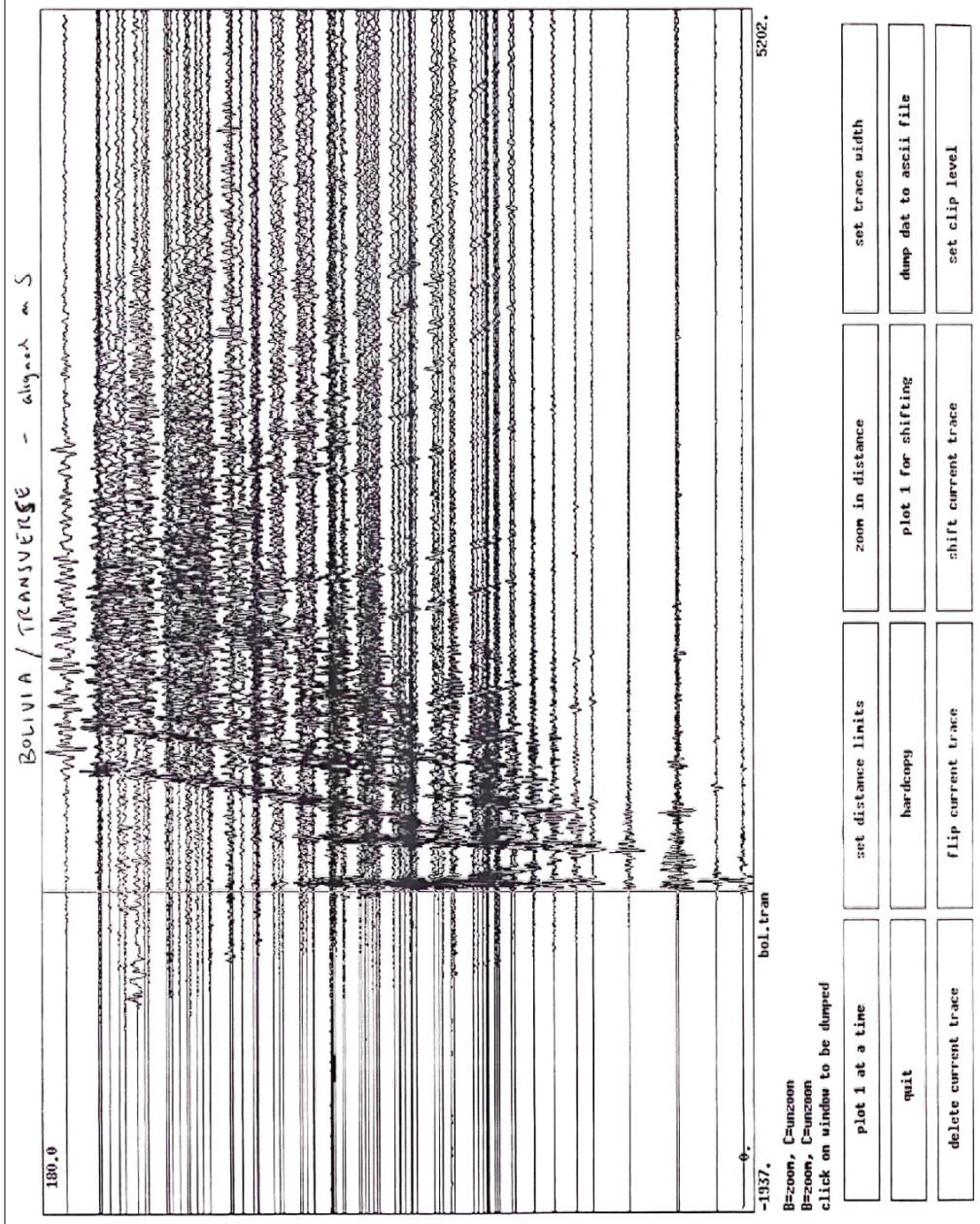

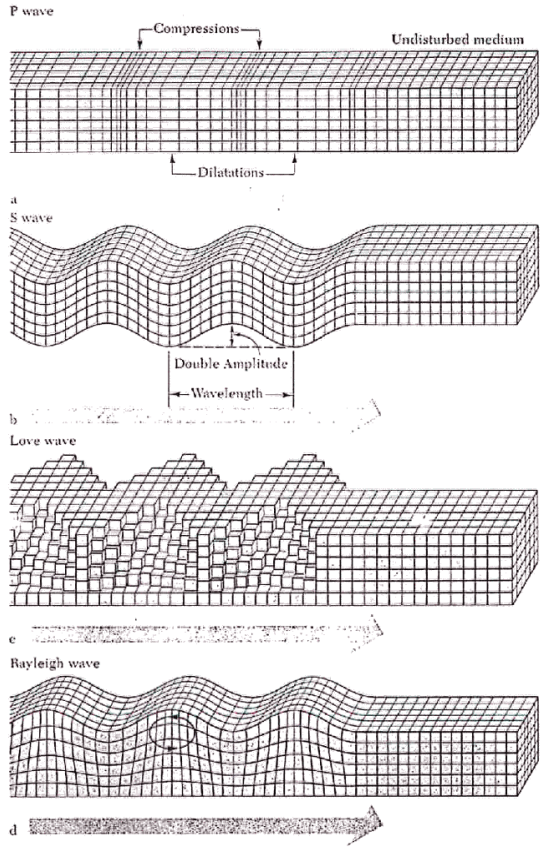

FIGURE 5
Diagram illustrating the forms of ground motion near the ground surface in four types of earthquake waves. [From Bruce A. Bolt, *Nuclear Explosions and Earthquakes*. W. H. Freeman and Company. Copyright © 1976.]

①

Ray Theory

Flat

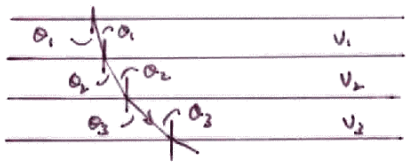

Snell's Law

$$\frac{1}{V_1}\sin\theta_1 = \frac{1}{V_2}\sin\theta_2 = \frac{1}{V_3}\sin\theta_3 = \cdots$$

Ray parameter

$$p = \frac{1}{V}\sin\theta = \frac{1}{V_{TP}}$$

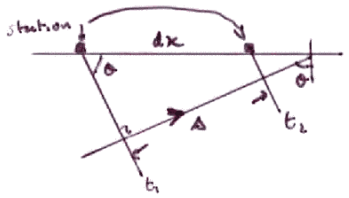

$$\Delta = \delta t \cdot v = \delta x \sin\theta$$

$$\therefore \frac{dT}{dx} = \frac{1}{V}\sin\theta = p$$

②

Spherical Earth

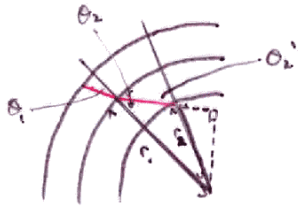

$\theta_2 \neq \theta_2'$

$$r_1 \sin\theta_2 = r_2 \sin\theta_2'$$

$$\therefore p = \frac{r}{v}\sin\theta = \frac{dT}{d\Delta} \quad \left(\frac{\text{seconds}}{\text{radian}}\right)$$

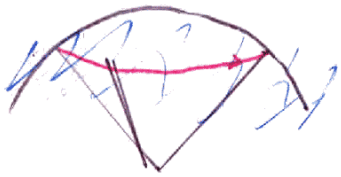

(3)

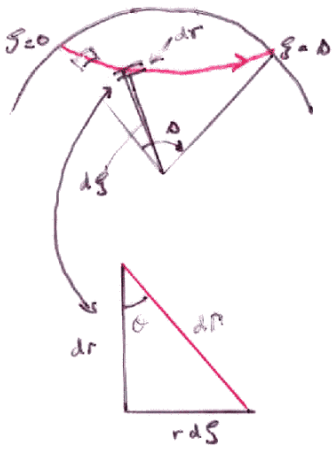

$$\sin\theta = r\frac{d\xi}{d\Gamma}$$

$$\therefore \quad d\Gamma = \frac{r^2}{pV}\,d\xi$$

$$T = \int_\Gamma \frac{1}{V}\,d\Gamma$$

$$\delta T = -\int_\Gamma \frac{\delta V}{V^2}\,d\Gamma \qquad \text{(Fermat)}$$

rewrite over distance

$$\delta T = \int_0^\Delta G(\xi)\,\delta v(\xi)\,d\xi$$

$$G(\xi) = -\frac{1}{V^2}\frac{d\Gamma}{d\xi} = -\frac{r^2}{pV^3}$$

Need to know $r(\xi)$ to get $v(\xi)$

Now $\tan\theta = r\frac{d\xi}{dr} = \frac{xp}{(1-(xp)^2)^{\frac{1}{2}}}$ $\therefore$ $\frac{d\xi}{dr} = \frac{p}{r}\left(\frac{r^2}{V^2}-p^2\right)^{-\frac{1}{2}}$

(4)

1D Earth

$$\frac{d\xi}{dr} = \frac{p}{r}\left(\frac{r^2}{V^2}-p^2\right)^{-\frac{1}{2}}$$

$$\therefore \quad \Delta = 2\int_{r_{TP}}^{R}\frac{d\xi}{dr}\,dr$$

$$\Delta = 2\int_{r_{TP}}^{R}\frac{p}{r}\left(\frac{r^2}{V^2}-p^2\right)^{-\frac{1}{2}}dr \qquad *$$

$$dT = \frac{d\Gamma}{V} = \frac{r^2}{pV^2}\,d\xi$$

$$\therefore \quad \frac{d\xi}{dr} = \frac{pV^2}{r^2}\frac{dT}{dr} \qquad \text{or} \qquad \frac{dT}{dr} = \frac{r^2}{pV^2}\frac{d\xi}{dr}$$

$$T = 2\int_{r_{TP}}^{R}\frac{dT}{dr}\,dr$$

$$= 2\int_{r_{TP}}^{R}\frac{r}{V^2}\left(\frac{r^2}{V^2}-p^2\right)^{-\frac{1}{2}}dr \qquad *$$

Square root singularity $\Rightarrow$ sensitivity to turning point structure

($p = \frac{r}{V}$ at TP)

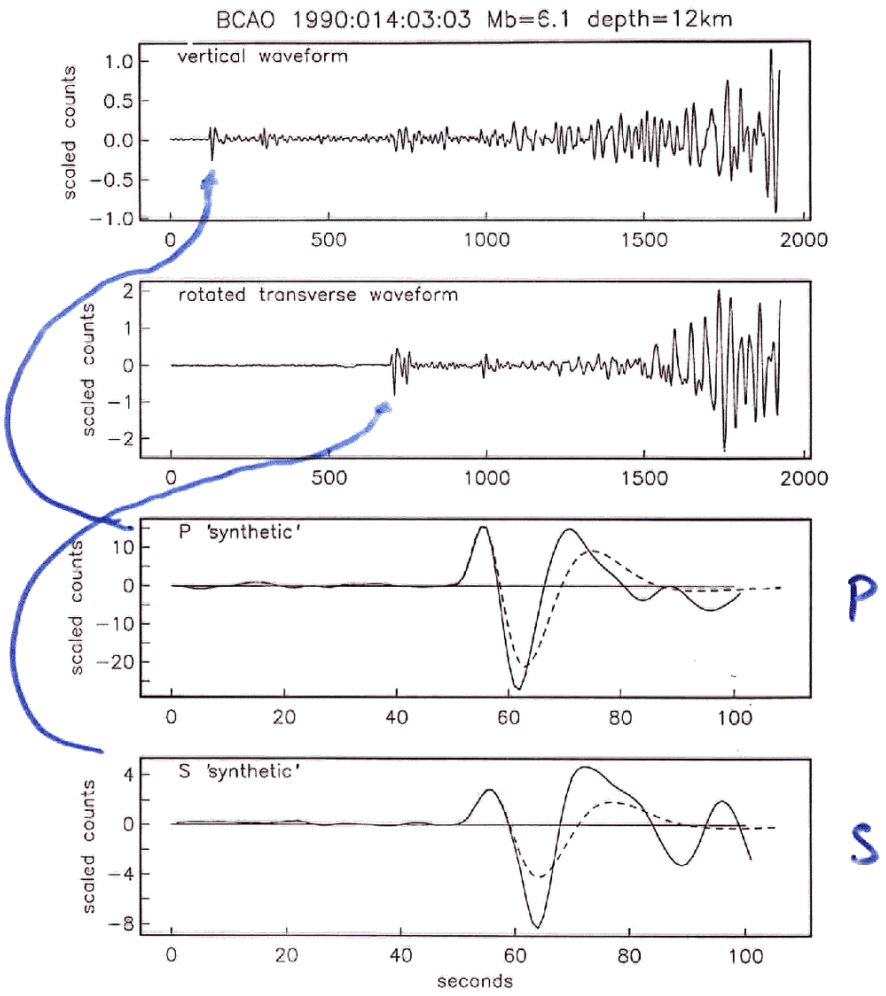

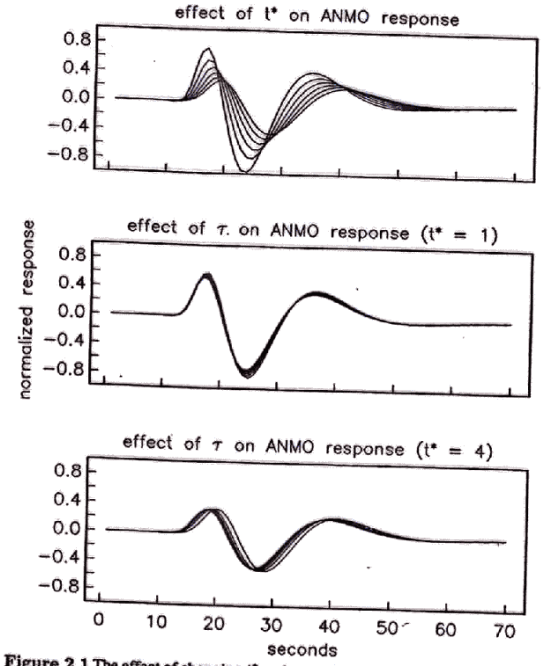

Figure 2.1 The effect of changing t^* and τ_1 on the absorption-band attenuation operator is illustrated. A change in τ_1 mainly causes a delay of the whole waveform. An increase in t^* leads to both a delay and a broadening.

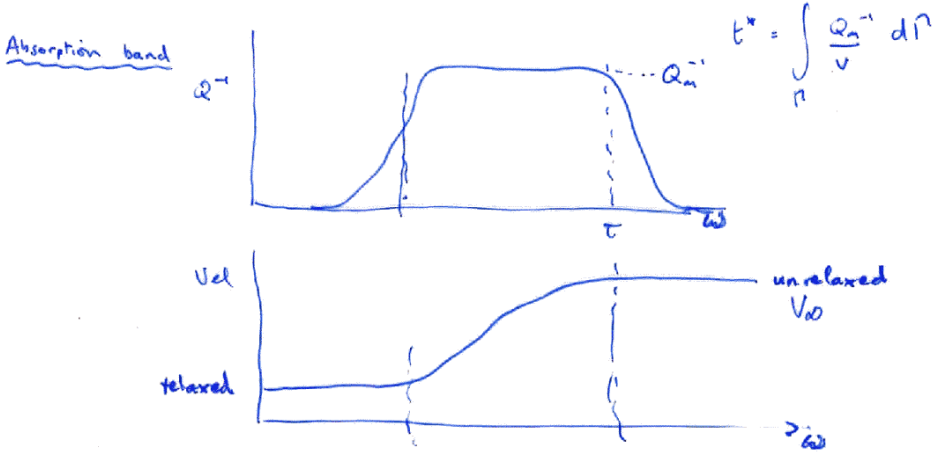

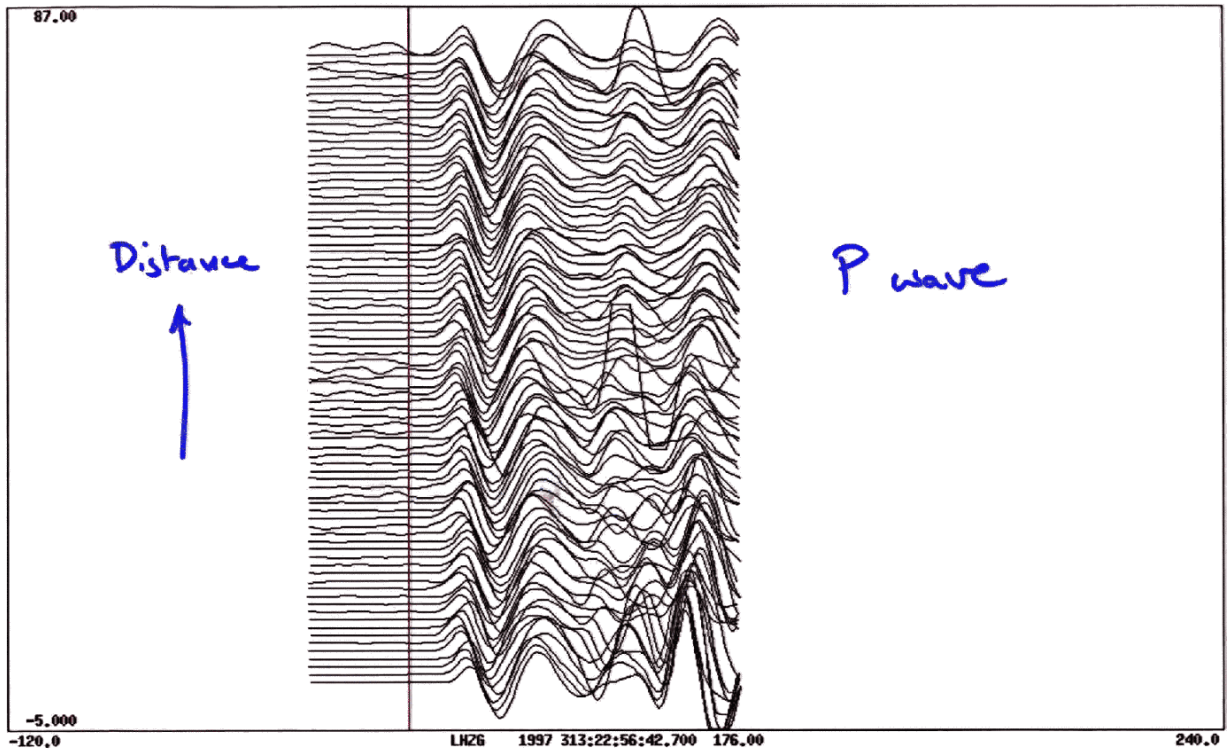
87.00
Distance
P wave
-5.000
-120.0
LHZG 1997 313:22:56:42.700 176.00
240.0
A=align, B=next, C=last
click on window to be dumped
dist/az
A:nshift B:rrmin C:snr
zoom in distance
set trace width
quit
hardcopy
A,B: next event, C: last event
dump dat to ascii file
set clip level
select one trace
A,B= align, C=plot raw data
dump data for cluster plot

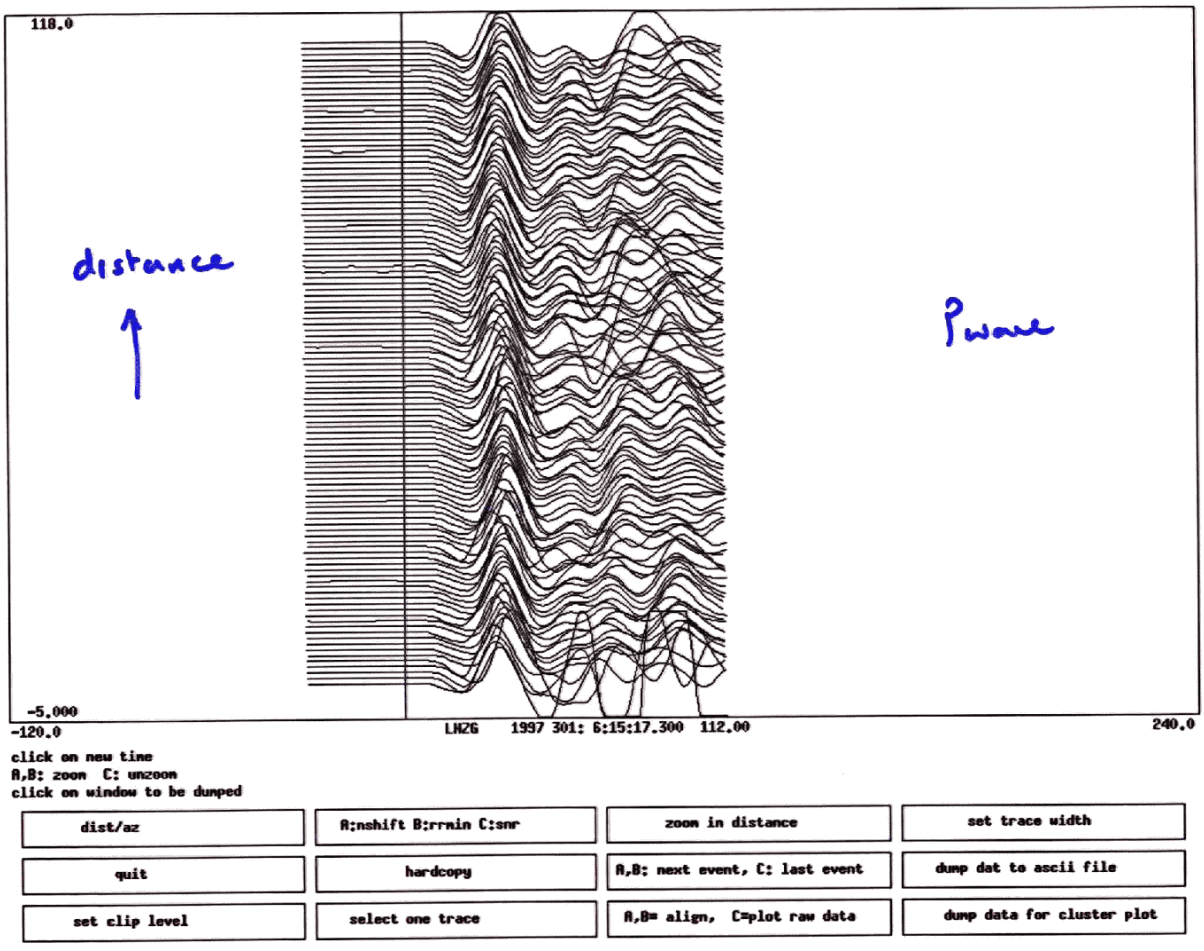
118.0
distance
Pwave
-5.000
-120.0
LHZG 1997 301: 6:15:17.300 112.00
240.0
click on new time
A,B: zoom C: unzoom
click on window to be dumped
dist/az
A:nshift B:rrmin C:snr
zoom in distance
set trace width
quit
hardcopy
A,B: next event, C: last event
dump dat to ascii file
set clip level
select one trace
A,B= align, C=plot raw data
dump data for cluster plot

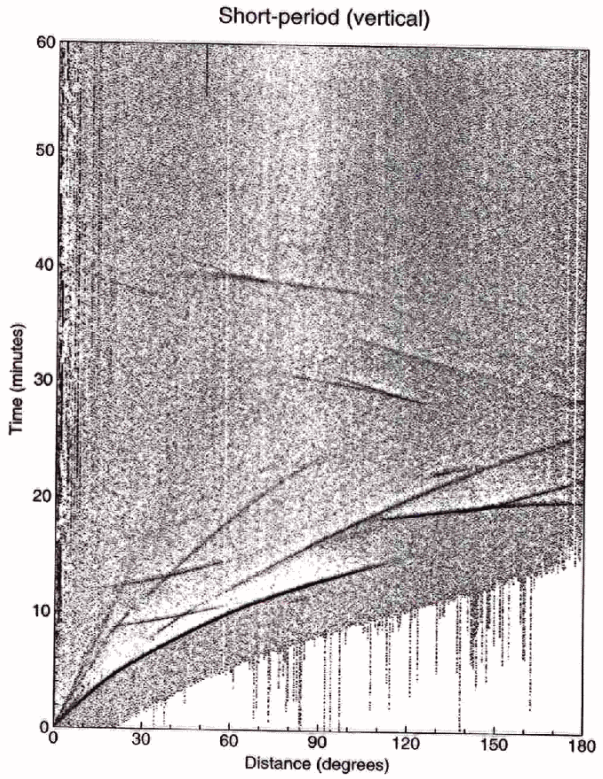

Fig. 4.18. A stack of short-period (<2 s), vertical component data from the global networks between 1988 to 1994. See Figure 4.19 for a key to the phase names. (From Astiz et al., 1996.)

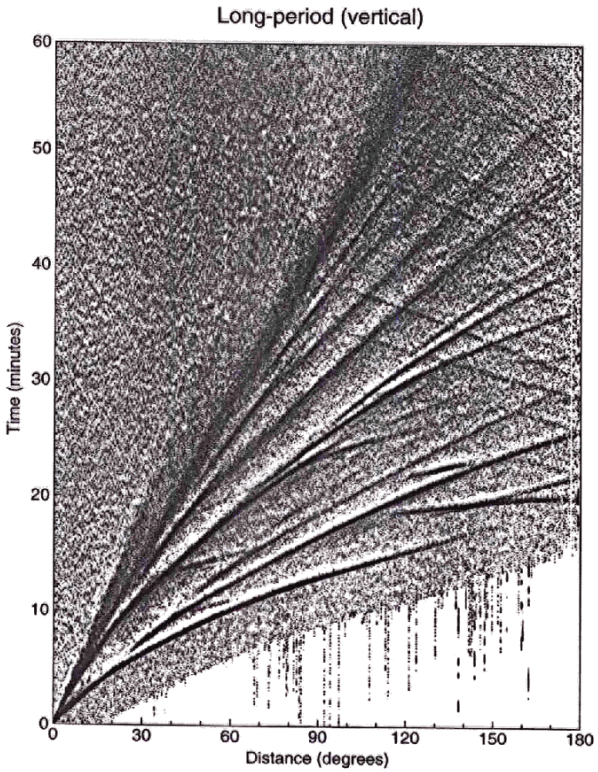

Fig. 4.20. A stack of long-period (>10 s), vertical component data from the global networks between 1988 to 1994. See Figure 4.23 for a key to the phase names. (From Astiz et al., 1996.)

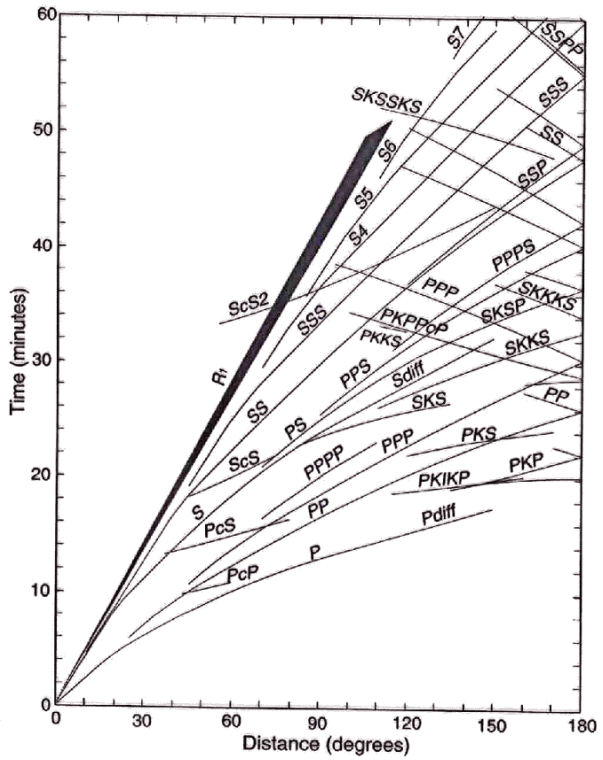

Fig. 4.23. The phases visible in the long-period stacks shown in Figures 4.20–4.22. Travel time curves are calculated using the IASP91 velocity model (Kennett and Engdahl, 1991). (From Astiz et al., 1996.)

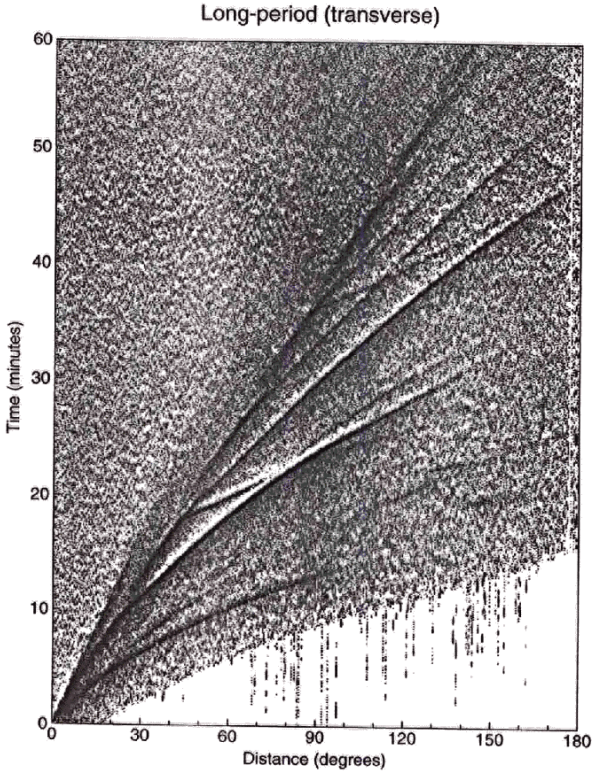

Fig. 4.22. A stack of long-period (> 10 s), transverse component data from the global networks between 1988 to 1994. See Figure 4.23 for a key to the phase names. (From Astiz et al., 1996.)

ISC travel times

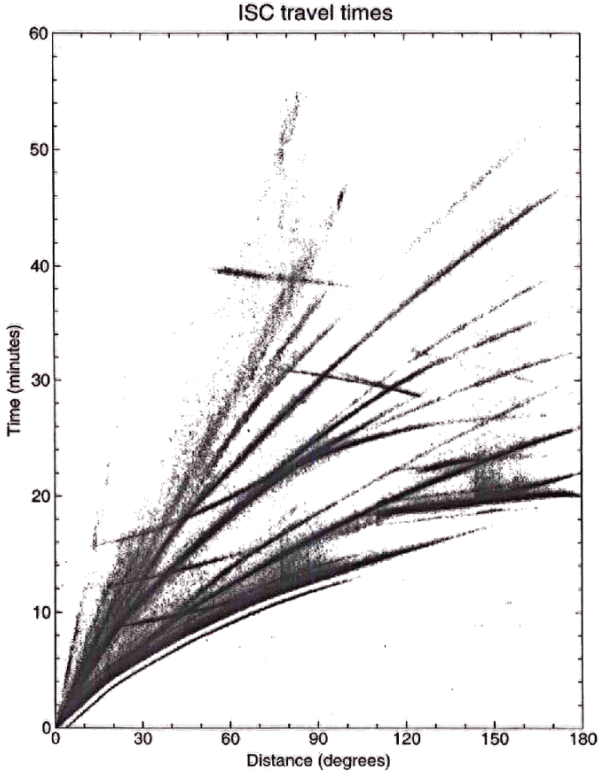

Time (minutes)

1 2 3 4 5 6

Fig. 4.17. Travel time picks collected by the ISC between 1964 and 1987 for events shallower than 50 km. Over five million individual picks are plotted, the bulk of which are *P*, *PKP*, and *S* arrivals. However, several later arriving branches can also be seen, including *PP*, *PKS*, *PcP*, *PcS*, *ScS*, *PKKP*, and *PKPPKP*. See Figures 4.19 and 4.23 for a key to the phase names. The phases visible at ±1 minute from the *P*-wave are due to errors in assigning times.

ISC S Travel Times Relative to PREM

Arrivals after identified ISC S (Jeffreys-Bullen ±7.5s) have been removed

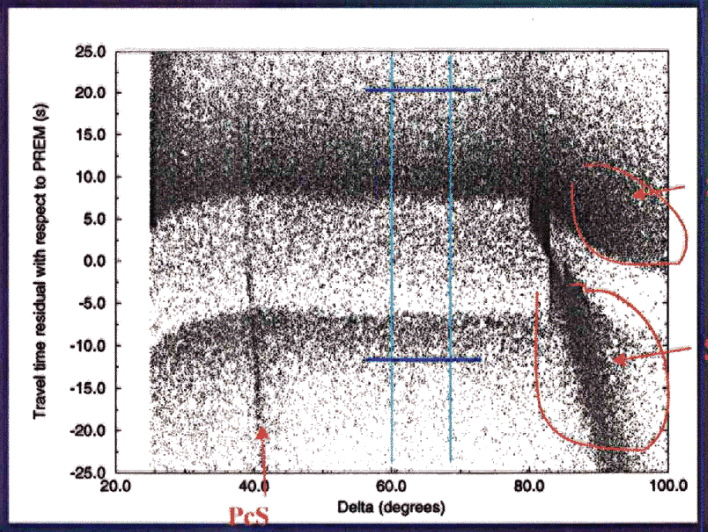

Data Binned in the 60-70° Epicentral Distance Range

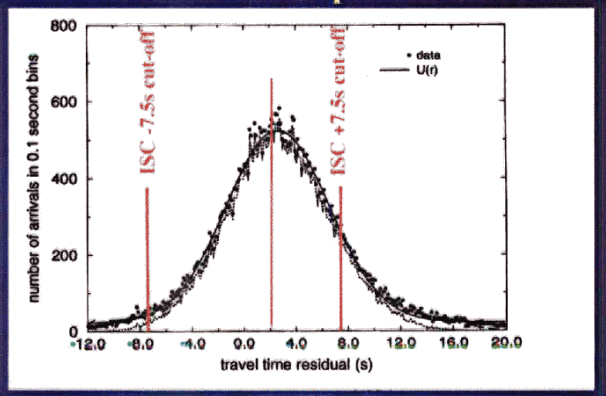

Modified from Robertson and Woodhouse, 1995